Progress In Electromagnetics Research M, Vol. 88, 33–44, 2020

Magnetically Controlled Electromagnetic Tunneling through Symmetric Trilayer Containing Ferrite Layer

Sergey A. Afanas'ev*, Irina V. Fedorova, and Dmitry I. Sementsov

Abstract—Tunneling of microwave radiation through a symmetrical trilayer ENG-ferrite-ENG is considered, where ENG refers to a medium of negative permittivity. Such a trilayer is an example of a magnetically controlled structure that under certain conditions allows a complete (or perfect) tunneling of the incident radiation. In this paper, the general conditions of perfect tunneling are analyzed, and the transmissive properties of the structure are studied numerically. It is demonstrated that a broad passband, in which the structure is almost completely transparent, may be obtained both above and below the frequency of the ferromagnetic resonance. The bandwidth can be effectively controlled by an external field that is magnetizing the ferrite layer.

1. INTRODUCTION

Nowadays, artificial composites, known as metamaterials, are engineered to have a wide diversity of electromagnetic properties [1–3]. The material constants of metamaterials — permittivity ε and permeability μ — can be either positive or negative. Metamaterials include double-negative (DNG) media with $\varepsilon < 0$, $\mu < 0$, and single-negative (SNG) media, which are divided into ε-negative, or ENG ($\varepsilon < 0$, $\mu > 0$) and μ-negative, or MNG ($\varepsilon > 0$, $\mu < 0$). Electromagnetic waves in SNG media are evanescent, so that the single SNG layers are opaque. However, the lossless multilayer structures containing SNG layers can be totally transparent under certain conditions. This phenomenon is known as the complete (or perfect) electromagnetic tunneling [3–5]. Typically, structures for the perfect tunneling are composed of alternating layers of ENG and MNG media, or DNG and DPS (double-positive) media [3–8], although many other combinations have been proposed in recent years [9–17]. One of the simplest combinations of layers is a symmetrical trilayer, for which the conditions of total transmission can be easily obtained analytically using the transfer matrix method [6, 7, 13, 14].

The perfect tunneling is a resonant phenomenon, which is associated with the enhancement of surface waves at the interfaces of the layers with contrast properties [5, 15]. Therefore, the layers must be composed into the structure in such a way that certain resonance conditions are met as precisely as possible. This suggests that it is possible to achieve the required correlations between the parameters of individual layers using external magnetic field. For microwaves, we suggest obtaining a magnetically tunable structure by inserting a layer of ferrite that is operated near the ferromagnetic resonance frequency. In this paper, we show that the tunneling of the microwave radiation through such a structure can be near-perfect if the low loss ferrite is used. As far as we know, the structures for the perfect tunneling containing ferrite layers have not been analyzed in current literature.

We consider a symmetric trilayer ENG-ferrite-ENG, where the ferrite layer is magnetized in-plane by an external magnetic field. The ferrite is an MNG medium in the cutoff region, i.e., at the frequencies of interval $f_{\rm r} < f < f_{\rm ar}$, where $f_{\rm r}$ and $f_{\rm ar}$ are the frequencies of the ferromagnetic resonance and anti-resonance, correspondingly. In the regions $f < f_{\rm r}$ and $f > f_{\rm ar}$, the ferrite appears as DPS material.

Received 9 September 2019, Accepted 19 November 2019, Scheduled 30 December 2019

* Corresponding author: Sergey Anatol'evich Afanas'ev (asa_rpe@mail.ru).

The authors are with the Department of Radiophysics and Electronics, Ulyanovsk State University, Ulyanovsk, Russia.

Accordingly, first we examine the resonant conditions of the perfect tunneling for symmetric lossless trilayers ENG-MNG-ENG and ENG-DPS-ENG. The required conditions were obtained in [13, 14] via the transfer matrix method. In contrast with [13, 14], we obtain and analyze all possible solutions of the corresponding equations in their most general form. Secondly, we apply these solutions to the lossy trilayer ENG-ferrite-ENG with a purpose to determine the optimal conditions for the near-perfect tunneling through the structure.

2. PROBLEM FORMULATION

The geometry of this problem is illustrated in Fig. 1 in the Cartesian coordinate system. We consider a symmetric trilayer structure placed in air. The thicknesses of its layers are $d_1/d_2/d_1$. Each layer is homogeneous and infinitely extended in the directions of x- and z-axes.

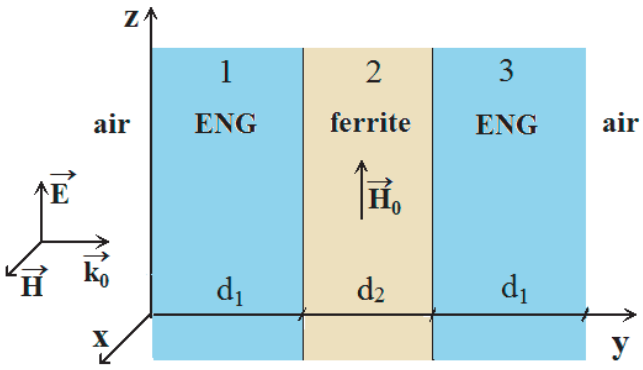

Figure 1. Geometry of the problem.

The outer layers 1 and 3 represent an ENG medium of negative permittivity. Further we assume that ENG medium is isotropic and has the permeability $\mu_1 = 1$. For its complex permittivity $\varepsilon_1 = \varepsilon_1' - i\varepsilon_1''$, we choose a simple Drude model of dispersion [9–11, 14–16, 18]:

$$\varepsilon_1 = 1 - \frac{\omega_p^2}{\omega\,(\omega - i\Gamma)}, \tag{1}$$

where $\omega = 2\pi f$ is a circular frequency; ω_p is the plasma circular frequency; and Γ is the damping frequency. For the constant parameters in Eq. (1), we select the values of $f_p = (\omega_p/2\pi) = 7\,\text{GHz}$ and $\Gamma = 10^{-3}\omega_p$. According to Eq. (1), the permittivity ε_1 has a negative real part $\varepsilon_1' < 0$ when $f < f_p$.

The inner layer 2 is a ferrite that is magnetized to the level of saturation by an external magnetic field $\mathbf{H}_0$ that is applied along z-axis. The magnetic gyrotropy of the ferrite is induced via the magnetizing field.

At microwave frequencies, the ferrite material is characterized by the scalar complex permittivity $\varepsilon_2 = \varepsilon_2' - i\varepsilon_2''$ and the permeability tensor [19]

$$\hat{\mu} = \begin{pmatrix} \mu & i\,\mu_a & 0 \\ -i\,\mu_a & \mu & 0 \\ 0 & 0 & 1 \end{pmatrix}, \tag{2}$$

$$\mu = \frac{\omega_H(\omega_M + \omega_H) - \omega^2}{\omega_H^2 - \omega^2}, \quad \mu_a = \frac{\omega\,\omega_M}{\omega_H^2 - \omega^2},$$

where $\omega_H = \gamma\mu_0 H_0$, $\omega_M = \gamma\mu_0 M_0$, γ is the gyromagnetic ratio; μ_0 is the vacuum permeability; and M_0 is the saturation magnetization. To account for the magnetic losses, we replace parameter ω_H in Eq. (2) with $\omega_H - i\gamma\Delta H$, where ΔH is the ferromagnetic resonance linewidth. In our calculations we use parameters of ferrite material with extremely low magnetic losses (single crystal films of yttrium-iron

garnet): $M_0 = 147\,\text{kA/m}$, permittivity $\varepsilon_2' = 14.8$, dielectric loss tangent $\text{tg}\delta = \varepsilon_2''/\varepsilon_2' = 2 \cdot 10^{-4}$ and $\Delta H = 80\,\text{A/m}$ [20].

We assume that a plane transverse (TEM) electromagnetic wave propagating along y-axis is normally incident onto the structure (see Fig. 1). It has the electric vector $\mathbf{E}$ parallel to z-axis, and its magnetic vector $\mathbf{H}$ is directed along x-axis. It is known [19] that for such a polarization of the electric field, when $\mathbf{E}$ vector is parallel to the $\mathbf{H}_0$ vector, the ferrite is characterized by the scalar effective permeability

$$\mu_\perp = \mu - \mu_a^2/\mu = \mu_\perp' - i\mu_\perp''. \tag{3}$$

The value of $\mu_\perp$ is strongly dependent on the frequency ω and the magnetic field H_0 in the vicinity of ferromagnetic resonance. Thus, the structure ENG-ferrite-ENG can be tunable with respect to the transmission of microwave radiation. The real $\mu_\perp'$ and imaginary $\mu_\perp''$ parts of the effective permeability in Eq. (3) are shown in Fig. 2 as functions of frequency. The function $\mu_\perp'(f)$ has two zeros: the first is at the ferromagnetic resonance frequency that is determined as [19]

$$f_\text{r} = (1/2\pi)\,\sqrt{\omega_H(\omega_M + \omega_H)}, \tag{4}$$

and the second one is at the point of antiresonance $f_\text{ar} = (1/2\pi)\,(\omega_M + \omega_H)$. The effective permeability $\mu_\perp$ is negative at the frequencies from f_r to f_ar and positive outside of this interval.

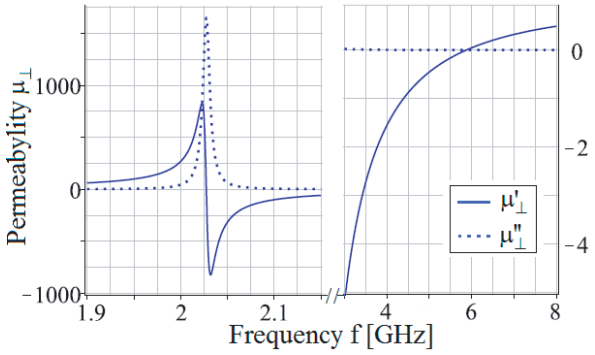

Figure 2. Real and imaginary parts of the effective permeability (3) versus frequency at $H_0 = 20\,\text{kA/m}$.

Throughout the paper, we use the values of H_0 that give $f_\text{ar} < f_p$. In such a case, the ENG-ferrite-ENG structure may be either ENG-MNG-ENG if $f_\text{r} < f < f_\text{ar}$ or ENG-DPS-ENG if the frequency belongs to the interval $f < f_\text{r}$ or $f_\text{ar} < f < f_\text{p}$. Further, we analyze both combinations in order to detect the possibility of an extremely high transmission of the incident electromagnetic energy through the structure, i.e., the near-perfect tunneling. Due to the small value of resonance linewidth ΔH, the magnetic losses of the ferrite are significant only in the neighborhood of f_r frequency (see the plot of $\mu_\perp''(f)$ dependence in Fig. 2). The dielectric losses of the ferrite and the ENG material are small enough, so the conditions of the perfect tunneling obtained for lossless structures can be used. In the next Section 3, we derive and analyze such conditions, assuming the structure to be lossless.

3. CONDITIONS OF PERFECT TUNNELING

The conditions of the perfect tunneling can be derived using the following procedure. Solving the boundary problem of electrodynamics for a given geometry, a unimodular field-transfer matrix of the structure can be obtained [18]. Assuming that wave fields are proportional to $\exp(i\omega t)$, the transfer matrices for the individual layers are written as

$$N_j = \begin{pmatrix} \cos(k_j d_j) & i\dfrac{k_j}{k_0\mu_j}\sin(k_j d_j) \\ i\dfrac{k_0\mu_j}{k_j}\sin(k_j d_j) & \cos(k_j d_j) \end{pmatrix}, \quad j = 1,\ 2,\ 3. \tag{5}$$

Here j denotes the number of layer according to Fig. 1; $k_0 = 2\pi f/c$ is the wave number in vacuum; c is the velocity of light in vacuum; the wave numbers k_j for SNG media are imaginary and equal to

$$k_j = -ik_0\sqrt{|\varepsilon_j\mu_j|}, \tag{6}$$

and they are real for DPS media:

$$k_j = k_0\sqrt{\varepsilon_j\mu_j}. \tag{7}$$

The transfer matrix of the symmetric trilayer structure under study is the product of the respective transfer matrices for the individual layers, $G = N_1N_2N_1$. Using the elements of matrix G, both the amplitude reflection coefficient

$$r = \frac{G_{11} + G_{12} - G_{21} - G_{22}}{G_{11} + G_{12} + G_{21} + G_{22}} \tag{8}$$

and the amplitude transmission coefficient

$$t = \frac{2}{G_{11} + G_{12} + G_{21} + G_{22}} \tag{9}$$

can be determined. Then the transmittance (energy transmission coefficient) can be calculated as $T = |t|^2$. The tunneling of the incident electromagnetic wave is perfect when $T = 1$. At the same time, in the absence of absorption, the reflectance $R = |r|^2$ must be equal to zero. Since the structure is placed in air, we determine that $G_{11} = G_{22}$. Thus, in accordance with Eq. (8), the criterion of perfect tunneling is obtained by equating the non-diagonal elements of matrix G to zero: $G_{12} = G_{21} = 0$.

3.1. Symmetric Structure ENG-MNG-ENG

Consider the lossless symmetric trilayer structure with the material parameters $(-\varepsilon_1, \mu_1)/(\varepsilon_2, -\mu_2)/(-\varepsilon_1, \mu_1)$, where $\varepsilon_{1,2}$ and $\mu_{1,2}$ are real positive numbers. The elements of the transfer matrix G obtained for such a trilayer are the following:

$$G_{11} = G_{22} = \cosh 2\varphi_1 \cosh\varphi_2 - \frac{1}{2}\left(\frac{Z_1}{Z_2} + \frac{Z_2}{Z_1}\right)\sinh 2\varphi_1 \sinh\varphi_2, \tag{10}$$

$$\begin{pmatrix} G_{12} \\ G_{21} \end{pmatrix} = \frac{i}{2Z_2}\begin{pmatrix} 1 \\ -1/Z_1^2 \end{pmatrix}\left[\begin{array}{c} 2Z_1Z_2\coth\varphi_2\sinh 2\varphi_1 + \begin{pmatrix} 1 \\ -1 \end{pmatrix}(Z_1^2 - Z_2^2) \\ -(Z_1^2 + Z_2^2)\cosh 2\varphi_1 \end{array}\right]\sinh\varphi_2.$$

Here $\varphi_{1,2} = k_0 n_{1,2} d_{1,2}$ are the optical thicknesses of the layers; $n_{1,2} = (\varepsilon_{1,2}\mu_{1,2})^{1/2}$ are the absolute values of refractive indexes; and $Z_{1,2} = (\mu_{1,2}/\varepsilon_{1,2})^{1/2}$ are the absolute values of layer impedances.

Applying the criterion $G_{12} = G_{21} = 0$ to Eq. (10), we get the further condition of the perfect tunneling:

$$\tanh\varphi_2 = \frac{2Z_1Z_2\sinh 2\varphi_1}{\eta\left(Z_1^2 - Z_2^2\right) + \left(Z_1^2 + Z_2^2\right)\cosh 2\varphi_1}, \tag{11}$$

where we denote $\eta = \left(1 - Z_1^2\right)/\left(1 + Z_1^2\right) = (\varepsilon_1 - 1)/(\varepsilon_1 + 1)$.

Equation (11) is solved numerically with respect to the variable μ_2 (it should be emphasized that we are only interested in the real positive solutions). Fig. 3 represents a typical view of the solved μ_2 as a function of frequency with fixed values of all other parameters found in Eq. (11).

One can see that Eq. (11) may have either one or two solutions depending on the frequency. The first solution $\mu_2^{(1)}$ exists at any frequency; its maximum value $\mu_2(0)$ is achieved in the low frequency limit. As the frequency increases, the value of $\mu_2^{(1)}$ falls smoothly, tending in the high frequency limit to the value of $\mu_2(\infty)$. The second solution $\mu_2^{(2)} < \mu_2^{(1)}$ emerges at frequencies $f > f_0$, its value increasing with the frequency, tending to the same limit $\mu_2(\infty)$ as the first solution $\mu_2^{(1)}$.

The values of $\mu_2(0)$, $\mu_2(\infty)$, and f_0 may be estimated analytically, using the appropriate approximations.

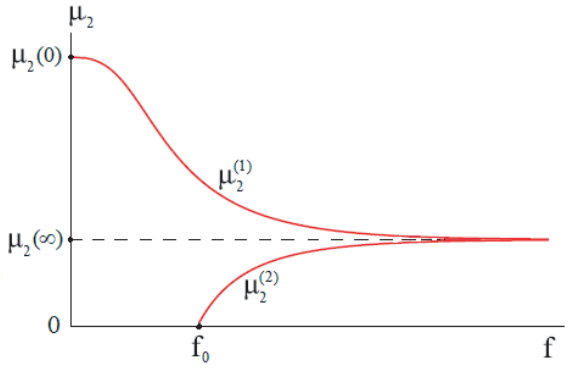

Figure 3. The solutions μ_2 of the Equation (11) versus frequency.

3.1.1. Low Frequency Limit

All three layers can be considered as optically thin ($\varphi_{1,2} \ll 1$), and we can allow for Eq. (11) $\tanh\varphi_2 \approx \varphi_2$, $\sinh 2\varphi_1 \approx 2\varphi_1$, $\cosh 2\varphi_1 \approx 1$. By doing this we obtain an approximate equation, which has the following solution

$$\mu_2(0) \approx 2\xi(\varepsilon_1 + 1) - \varepsilon_2 \tag{12}$$

or

$$\mu_2(0) \approx \varepsilon_2 \left(\frac{\xi}{\xi_{\min}} - 1 \right), \tag{13}$$

where the dimensionless parameter $\xi = d_1/d_2$ (thickness ratio) is introduced, and

$$\xi_{\min} = \frac{\varepsilon_2}{2(\varepsilon_1 + 1)}. \tag{14}$$

Therefore, at low frequencies the solution $\mu_2^{(1)}$ is weakly dependent on the frequency, tending to the limit value (12), which is linearly dependent on the thickness ratio ξ. The expression (13) shows that positive solutions exist only when the thickness ratio is sufficiently high ($\xi > \xi_{\min}$), where the value of $\xi_{\min}$ is determined by the layers' permittivities.

3.1.2. High Frequency Limit

Noting that $|\eta| < 1$, the first term in the denominator of the right side of Equation (11) can be neglected. Consequently, keeping in mind that when $\varphi_{1,2} \to \infty$ we have $\tanh\varphi_2 = \tanh 2\varphi_1 \approx 1$ we obtain

$$\mu_2(\infty) = \varepsilon_2/\varepsilon_1. \tag{15}$$

3.1.3. Estimation of f_0

Near the frequency f_0 $\mu_2 \to 0$, and we can assume $\tanh\varphi_2 \approx \varphi_2$. As a consequence, we conclude that the frequency f_0, which gives $\mu_2^{(2)} = 0$, can be found as the solution of the following equation:

$$k_0 Z_1 \varepsilon_2 d_2 (\eta + \cosh 2\varphi_1) = 2 \cdot \sinh 2\varphi_1. \tag{16}$$

A rough estimation of f_0 can be made using Eq. (16), by assuming that with a sufficiently large φ_1 we have $\sinh 2\varphi_1 \approx \cosh 2\varphi_1 \gg \eta$ and, therefore,

$$f_0 \approx \frac{c}{\pi Z_1 \varepsilon_2 d_2} = \frac{c\sqrt{\varepsilon_1}}{\pi \varepsilon_2 d_2}. \tag{17}$$

The conclusion is that the frequency f_0 increases with permittivity ε_1, decreases with d_2, and has relatively weak dependence on d_1 (or parameter ξ).

The results of the accurate numerical solution of Equation (11) are represented in Fig. 4. The frequency dependencies of the solutions μ_2 depicted in Fig. 4 were obtained with fixed values of ε_1,

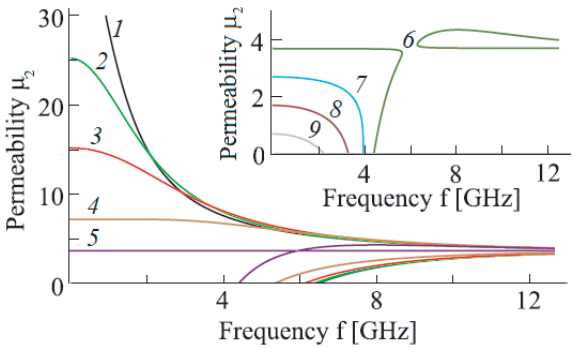

Figure 4. The solutions μ_2 of the Equation (11) versus frequency at $\varepsilon_1 = 4$, $\varepsilon_2 = 14.8$, $d_2 = 2\,\text{mm}$, $\xi = 6,\ 4,\ 3,\ 2.2,\ 1.85,\ 1.84,\ 1.75,\ 1.65,\ 1.55$ (curves 1–9).

ε_2, and d_2, and with different values of the ξ parameter. Data used in the calculations of Fig. 4 yield $\mu_2(\infty) = 3.7$, $\xi_{\min} = 1.48$, $f_0 \approx 6.45\,\text{GHz}$ (the latter is the rough estimation by Eq. (17) disregarding the dependence on ξ).

One can see that the plots of $\mu_2(f)$ dependencies are of the "standard" view depicted in Fig. 3 with only sufficiently large values of ξ lying above a definite "critical" value (curves 1–4). Curve 5 corresponds to that "critical" value, which equals to

$$\xi_{\text{cr}} = \frac{\varepsilon_2}{2\varepsilon_1} = \frac{1}{2}\mu_2(\infty). \tag{18}$$

At $\xi = \xi_{\text{cr}}$, $\mu_2(0) = \mu_2(\infty)$ and the solution $\mu_2^{(1)}$ is frequency independent. The condition (18) of perfect tunneling, known as the "matched trilayer condition" [13], is a specific case derived from more general condition (11).

Within the interval of $\xi_{\min} < \xi < \xi_{\text{cr}}$, the shape of $\mu_2(f)$ dependencies changes noticeably. Namely, the plot splits into two branches (as curve 6 shows), and there is a frequency interval that has no solution. With a further decrease of ξ, the second branch is shifted to the region of extremely high frequencies, and there is only one solution that can be observed (the curves 7–9). It is localized in the limited interval of low frequencies, restricted above by the frequency that is similar to the frequency f_0 and also can be found with sufficient accuracy as the solution of Equation (16).

3.2. Symmetric Structure ENG-DPS-ENG

Consider a symmetric trilayer of material parameters $(-\varepsilon_1, \mu_1)/(\varepsilon_2, \mu_2)/(-\varepsilon_1, \mu_1)$, where $\varepsilon_{1,2}$ and $\mu_{1,2}$ are real positive numbers. Now the elements of matrix G are

$$G_{11} = G_{22} = \cosh 2\varphi_1 \cos\varphi_2 - \frac{1}{2}\left(\frac{Z_1}{Z_2} - \frac{Z_2}{Z_1}\right)\sinh 2\varphi_1 \sin\varphi_2, \tag{19}$$

$$\begin{pmatrix} G_{12} \\ G_{21} \end{pmatrix} = \frac{i}{2Z_2}\begin{pmatrix} 1 \\ -1/Z_1^2 \end{pmatrix}\left[\begin{array}{c} 2Z_1Z_2\cot\varphi_2\sinh 2\varphi_1 + \begin{pmatrix} 1 \\ -1 \end{pmatrix}(Z_1^2 + Z_2^2) \\ -(Z_1^2 - Z_2^2)\cosh 2\varphi_1 \end{array}\right]\sin\varphi_2,$$

where all designations are the same as above in Section 3.1. Correspondingly, the perfect tunneling condition is written as

$$\tan\varphi_2 = \frac{2Z_1Z_2\sinh 2\varphi_1}{\eta\left(Z_1^2 + Z_2^2\right) + \left(Z_1^2 - Z_2^2\right)\cosh 2\varphi_1}. \tag{20}$$

Figure 5 represents an example of graphical solution of Equation (20) with respect to μ_2 variable. The left-hand side X and right-hand side Y of the equation are plotted versus square root of μ_2. Note that the function $Y(\mu_2)$ has a discontinuity point at

$$\mu_2 = \mu_Y = \frac{\varepsilon_2}{\varepsilon_1}\frac{\cosh 2\varphi_1 + \eta}{\cosh 2\varphi_1 - \eta}. \tag{21}$$

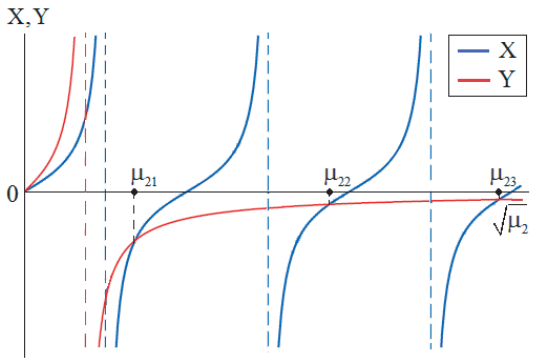

Figure 5. Graphical solution of the Equation (20).

Here Y is positive within the interval of $(0, \mu_Y)$ and negative when $\mu_2 > \mu_Y$, vanishing if $\mu_2 \to \infty$. The tangent function in the left-handed side has zeros at

$$\mu_2 = \mu_{0X}(m) = \frac{1}{\varepsilon_2}\left(\frac{\pi m}{k_0 d_2}\right)^2, \quad m = 1,\ 2,\ \ldots, \tag{22}$$

and discontinuities at

$$\mu_2 = \mu_X = \frac{1}{\varepsilon_2}\left(\frac{\pi}{k_0 d_2}\right)^2 \left(m - \frac{1}{2}\right)^2. \tag{23}$$

There exists an infinite set of solutions of Equation (20). Each solution μ_{2m} of order m is localized in the interval of $[\mu_{0X}(m-1),\ \mu_{0X}(m)]$. Within the framework of Fig. 5, one can see the solutions of the first three orders $m = 1,\ 2,\ 3$, which correspond to the intersection points of the negative branch of the function $Y(\mu_2)$ with three negative branches of the tangent function $X(\mu_2)$. One can see that the values of μ_{2m} are close to the corresponding zeros of the tangent function and, therefore, the expression (22) can be used for their rough estimation. In addition, we should note that depending on the position of the discontinuity point μ_Y, the intersection of the positive branches of the functions X and Y is possible. Moreover, one of the solutions may be absent.

Figure 6(a) shows the frequency dependences of the solutions μ_{2m} of several orders m for fixed values of ε_1 and ξ, and two different values of the thickness d_2. The plot represents a set of separate branches, and each of them corresponds to a specific value of m. It is seen that as the thickness d_2 decreases, the branches are shifted to higher frequencies. For the orders $m \geq 2$, the values of μ_{2m} decrease with frequency, vanishing if $f \to \infty$. At the same time, the solutions of the order $m = 1$ are localized in the frequency interval, restricted above by some limit frequency. In addition, the shape of dependence $\mu_{21}(f)$ may be different, as one can see in Fig. 6(b).

Figure 6(b) depicts the frequency dependences of the solution μ_{21} for a fixed value of the permittivity ε_1 and the thickness d_2, but for different values of the thickness ratio ξ. If $\xi < \xi_{\text{cr}}$ (according to (17), $\xi_{\text{cr}} = 1.85$) the dependence is increasing (the curves 3–5), and if $\xi \geq \xi_{\text{cr}}$ it is decreasing (the curves 1 and 2). When $\xi > \xi_{\min}$ (where $\xi_{\min}$ is determined, as before, by Eq. (14) and equals $\xi_{\min} = 1.48$), the frequency domain of existence of the root μ_{21} is restricted not only from above, but also from below (by a non-zero value).

4. TRANSMITTANCE OF ENG-FERRITE-ENG STRUCTURE

In this section, we assume that layers 1 and 3 are made of an ENG material, which is lossy and dispersive in accordance with Eq. (1). Also, layer 2 is a magnetized ferrite, and in the calculations we take into account its dielectric and magnetic losses. So, the material parameters of the layers (the permittivities ε_1, ε_2 and permeability $\mu_2 = \mu_\perp$) are considered here as complex numbers. In addition, when solving numerically Equations (11) and (20) in this Section, we take into account the dispersion of permittivity ε_1.

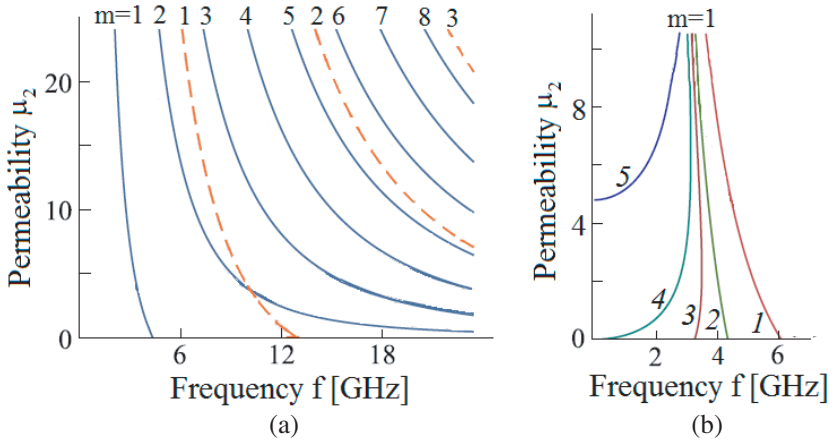

Figure 6. The solutions μ_2 of the Equation (20) versus frequency at $\varepsilon_1 = 4$, $\varepsilon_2 = 14.8$: (a) the solutions for different m at $\xi = 10$, $d_2 = 3$, 1 mm (solid and dashed lines); (b) the solution of order $m = 1$ at $d_2 = 2$ mm, $\xi = 3,\ 1.84,\ 1.65,\ 1.48,\ 1$ (curves 1–5).

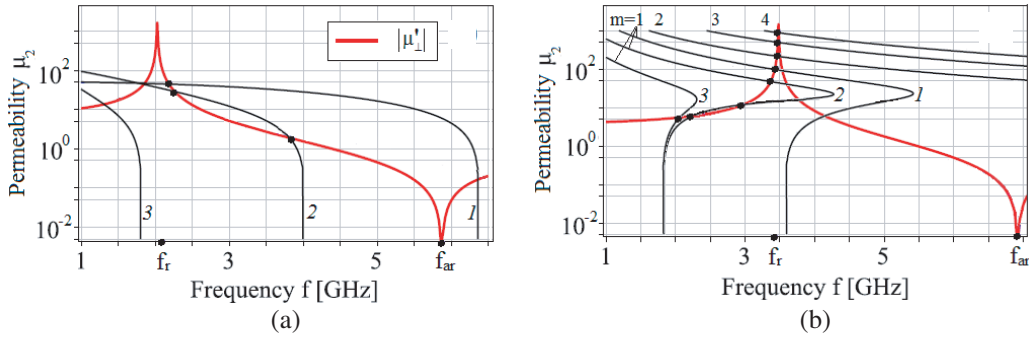

Figure 7. The effective ferrite permeability for (a) $H_0 = 20$ and (b) 50 kA/m and the solutions of the perfect tunneling conditions versus frequency: (a) ENG-MNG-ENG structure with $d_2 = 0.5$ mm, $\xi = 8,\ 2.5,\ 0.5$ (curves 1–3); (b) ENG-DPS-ENG structure: the solution of $m = 1$ with $d_2 = 1$ mm, $\xi = 2$ (1), $d_2 = 1.5$ mm, $\xi = 0.5$ (2), $d_2 = 2.5$ mm, $\xi = 0.5$ (3) and the solutions of $m = 2,\ 3,\ 4$ with $d_2 = 1.5$ mm, $\xi = 0.5$.

In Fig. 7, the absolute value of the real part $\mu'_\perp$ of the effective permeability in Eq. (3) of ferrite is plotted (using a logarithmic scale) versus the frequency. To reveal the possibility of the near-perfect tunneling through this structure, we overlay on these plots the solutions of Equations (11) and (20). At each intersection point with the plot of $|\mu'_\perp|(f)$ dependency there must exists the frequency of transmittance peak with magnitude of T close to unity.

Figure 7(a) shows the solutions of Equation (11) for the ENG-MNG-ENG structure, and we must look for intersections with the plot of $|\mu'_\perp|(f)$ in the region of $f_\mathrm{r} < f < f_\mathrm{ar}$. Based on the discussion in Section 3.1, it follows that there are three possible options. If $f_0 > f_\mathrm{ar}$, there can be only one intersection point lying in the described region (curve 1). If $f_0 < f_\mathrm{ar}$ and $\xi > \xi_\mathrm{min}$, there can be two intersections (curve 2), but there may be no intersection points (as for curve 3). It should be noted that for a structure with fixed parameters, the situation could be easily changed using the external magnetic field H_0. A change in its magnitude shifts the points of resonance and antiresonance, as well as the width of the interval $f_\mathrm{r} < f < f_\mathrm{ar}$ is controlled.

Figure 7(b) shows the solutions of Equation (20) for the ENG-DPS-ENG structure. As for the solution μ_{21} of the first order, three curves are shown for different sets of structure parameters. The curves for the solutions of the order $m \geq 2$ may have only one point of intersection with the plot of $|\mu'_\perp|(f)$ in the region of $f < f_\mathrm{r}$. This is also characteristic of the case $m = 1$ (curve 1). But if the

specific conditions are met, such as the values of $\xi < 1$, one can obtain more than one transmission peak corresponding to $m = 1$. This situation is illustrated by curve 2, which has three intersection points. The data used for curve 3 give one intersection point again, but it is located far from the resonant frequency, where the structure is nearly lossless.

The transmittance T of ENG-ferrite-ENG structure is determined using the transfer matrix method for the trilayer, as described in Section 3. A distinction consists of the complexity of the material parameters $\varepsilon_1, \varepsilon_2, \mu_2$. Therefore, the complex wave numbers in Eq. (5) are now determined by

$$k_j = k'_j - ik''_j = \pm k_0\sqrt{\varepsilon_j\mu_j}, \quad j = 1,\ 2,\ 3. \tag{24}$$

The sign of square root in Eq. (24) is chosen so that the imaginary part k''_2 is positive, which corresponds to the absorbing media.

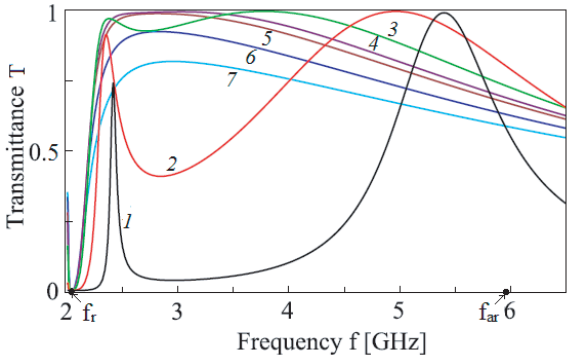

Figure 8. The transmittance of ENG-ferrite-ENG structure versus frequency at $H_0 = 20\,\text{kA/m}$, $d_2 = 1\,\text{mm}$, $\xi = 10,\ 5,\ 2.5,\ 1.8,\ 1.5,\ 1,\ 0.5$ (curves 1–7).

Figure 8 shows the $T(f)$ dependences calculated for different values of the thickness ratio ξ with the fixed values of the magnetizing field and all other parameters of the structure. For comparatively large ξ (curves 1–3), there are two well resolved peaks of the transmittance, which correspond to the solutions $\mu_2^{(1)}$ and $\mu_2^{(2)}$ of Equation (11). (Under certain conditions, the right peak may be found in the region $f > f_{\text{ar}}$ of positive $\mu'_\perp$, where it corresponds to the first order solution μ_{21} of Equation (20)). The left peak is located close to the resonant frequency and its position weakly depends on ξ. As the value of ξ decreases, the right peak shifts toward the resonant frequency, and the following changes occur:

- the peak value of the transmittance approaches unity;
- the peak broadening is observed, and due to the overlapping of the two peaks, the transmittance in the region between them gets higher;
- eventually, the region between two close peaks takes a form of a "plateau" with an almost constant transmittance of more than 0.99 (curve 4).

It should be noted that the value of $|\varepsilon'_1|$ in the center of a "plateau" ($|\varepsilon'_1| \approx 4.2$ at $f \approx 3\,\text{GHz}$) is such that the value of $\xi = 1.8$ taken for curve 4 is about "critical" value ξ_{cr}, given by Eq. (18). It means that one can get the maximum bandwidth of the near-perfect tunneling if the structure within the passband behaves as a "matched trilayer".

For smaller values of ξ, the peaks keep shifting towards each other; the width of the "plateau" decreases, and at a certain value $\xi = 1.5$ (curve 5) it contracts to a point. With smaller ξ, the solutions of Eq. (11) in the region of $\mu'_\perp < 0$ cannot be detected. Also, a weakly pronounced, broadened peak of transmittance with maximum value that is significantly less than unity (curves 6, 7) is observed.

The transmittance of ENG-ferrite-ENG structure can be easily controlled by a magnetizing field. If the field H_0 is varied, the shape of $T(f)$ dependencies realized at various values of d_2 and ξ, is generally preserved. In Fig. 9 $T(f)$ dependences are plotted at three different values of H_0 for two sets of structure parameters.

Figure 9(a) shows a passband of the near-perfect tunneling in the region $f_{\text{r}} < f < f_{\text{ar}}$ of negative effective permeability of the ferrite. As we demonstrated before, there can be two peaks of the

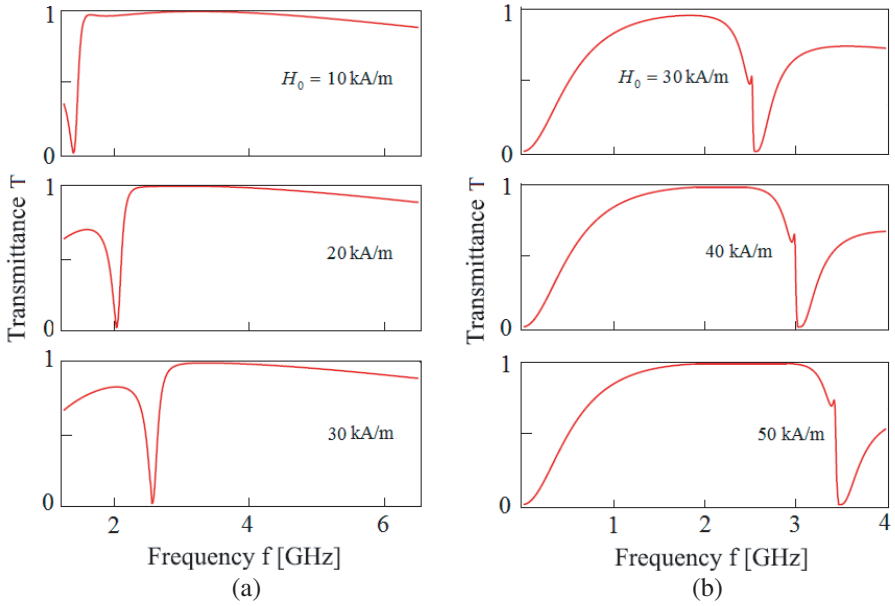

Figure 9. The transmittance of ENG-ferrite-ENG structure versus frequency for different values of the magnetizing field H_0: (a) $\xi = 1.8$, $d_2 = 0.5$ mm; (b) $\xi = 0.5$, $d_2 = 1$ mm.

transmittance. At $H_0 = 10$ kA/m the near-perfect tunneling is connected with the right peak of higher frequency. As the field H_0 increases, the passband initially becomes wider due to increased transmission between two separate peaks, but then becomes narrower.

In Fig. 9(b) one can see several regions of high transmittance positioned in the frequency region of $f < f_r$. As shown above, there may be multiple peaks corresponding to the solutions μ_{2m} of perfect tunneling condition (20) for ENG-DPS-ENG trilayer. However, the solutions with $m \geq 2$ are located in the immediate vicinity of the resonant frequency. Due to the high magnetic losses in this region and the peaks' proximity to each other, only a limited number of peaks are resolved. Also, the peak values of transmittance are usually small. The only exception is the peak corresponding to the first order solution, which is the most remote from resonant frequency. In Fig. 9(b), the peaks of orders $m \geq 2$ are not observed at all. The narrow peak corresponding to $m = 1$ is well resolved, but the transmittance at its maximum is low. When the magnetized field is sufficiently high, two additional solutions of order $m = 1$ can appear far enough from resonant frequency. Such a situation has been illustrated above by curve 2 in Fig. 7(b). Consequently, a wide passband of the near-perfect tunneling ($T \approx 0.997$) is formed with a "plateau" between two peaks of the transmittance (see the plot for $H_0 = 50$ kA/m in Fig. 9(b)).

5. CONCLUSION

In this paper, we have theoretically examined the transmission of a plane TEM wave through a symmetric trilayer structure that consists of two identical layers of ENG metamaterial and a ferrite layer between them. The ferrite layer is magnetized by an external magnetic field, in order for the transmissive properties of the structure under study can be magnetically controlled. Due to the presence of the layers with negative permittivity, the incident wave tunnels through the structure and the tunneling can be near-perfect if some specific conditions are met. The perfect tunneling conditions for the described structure were derived, and all possible solutions of the corresponding equations were analyzed.

The transmittance of the structure has been calculated using the transfer matrix method for the case of normal incidence while accounting the losses in the ferrite material (yttrium-iron garnet). Far enough from the ferromagnetic resonance frequency, the losses are negligibly small. We have shown that the structure can act as a bandpass filter of a broad bandwidth. The passband is restricted on both sides by two maxima of transmittance with the peak magnitude nearly equaling unity. The positions of these

two maxima are determined by the criteria of the perfect tunneling. In order to get the near-perfect tunneling throughout the entire passband, the parameters of the trilayer must be matched in a certain way. The passband can be located both above and below the ferromagnetic resonance frequency and its position and bandwidth can be effectively controlled by a magnetizing field.

ACKNOWLEDGMENT

The work was supported by the Ministry of Education and Science of the Russian Federation within the framework of the State task No. 3.6825.2017/BCH and RFFI (agreement No. 18-42-730001/18).

REFERENCES

1. Caloz, C. and T. Ito, *Electromagnetic Metamaterials: Transmission Line Theory and Microwave Applications*, John Wiley & Sons, New York, 2006.
2. Boltasseva, A. and V. M. Shalaev, "Fabrication of optical negative-index metamaterials: Recent advances and outlook," *Metamaterials*, Vol. 2, No. 1, 1–17, 2008.
3. Marques, R., F. Martin, and M. Sorolla, *Metamaterials with Negative Parameters: Theory, Design, and Microwave Applications*, Wiley, New York, 2008.
4. Alu, A. and N. Engheta, "Pairing an epsilon-negative slab with a mu-negative slab: Resonance, tunneling and transparency," *IEEE Transactions on Antennas and Propagation*, Vol. 51, No. 10, 2558–2571, 2003.
5. Baena, J. D., L. Jelinek, R. Marques, and F. Medina, "Near-perfect tunneling and amplification of evanescent electromagnetic waves in a waveguide filled by a metamaterial: Theory and experiments," *Phys. Rev. B*, Vol. 72, 075116, 2005.
6. Tan, W., Z. Wang, and H. Chen, "Complete tunneling of light through mu-negative media," *Progress In Electromagnetics Research M*, Vol. 8, 27–37, 2009.
7. Sabah, C., H. Tugrul Tastan, F. Dincer, K. Delihacioglu, M. Karaaslan, and E. Unal, "Transmission tunneling through the multilayer double-negative and double-positive slabs," *Progress In Electromagnetics Research*, Vol. 138, 293–306, 2013.
8. Afanas'ev, S. A., D. I. Sementsov, and Y. V. Yakimov, "Perfect tunneling of obliquely-incident wave through a structure with a double-negative layer," *Optics Communications*, Vol. 369, 164–170, 2016.
9. Feng, T., Y. Li, H. Jiang, Y. Sun, L. He, H. Li, Y. Zhang, Y. Shi, and H. Chen, "Electromagnetic tunneling in a sandwich structure containing single negative media," *Phys. Rev. E*, Vol. 79, 026601, 2009.
10. Zhou, L., W. Wen, C. T. Chan, and P. Sheng, "Electromagnetic-wave tunneling through negative-permittivity media with high magnetic fields," *Phys. Rev. Lett.*, Vol. 94, 243905, 2005.
11. Castaldi, G., I. Gallina, V. Galdi, A. Alu, and N. Engheta, "Electromagnetic tunneling through a single-negative slab paired with a double-positive bilayer," *Phys. Rev. B*, Vol. 83, No. 8, 081105, 2011.
12. Castaldi, G., V. Galdi, A. Alu, and N. Engheta, "Electromagnetic tunneling of obliquely incident waves through a single-negative slab paired with a double-positive uniaxial slab," *Journal of the Optical Society of America B*, Vol. 28, No. 10, 2362–2368, 2011.
13. Cojocaru, E., "Electromagnetic tunneling in lossless trilayer stacks containing single-negative metamaterials," *Progress In Electromagnetics Research*, Vol. 113, 227–249, 2011.
14. Chao, Y. and H. Zhao, "Electromagnetic tunneling through a three-layer asymmetric medium containing epsilon-negative slabs," *Central European Journal of Physics*, Vol. 11, No. 5, 594–600, 2013.
15. Zheng, J., Y. Chen, Z. Chen, X. Wang, P. Han, Z. Yong, Y. Wang, C. W. Leung, and C. M. Soukoulis, "Investigation of interface states in single-negative metamaterial layered structures based on the phase properties," *Optics Express*, Vol. 21, No. 14, 16742–16752, 2013.

16. Chen, Y., S. Huang, X. Yan, and J. Shi, "Electromagnetic tunneling through conjugated single-negative metamaterial pairs and double-positive layer with high-magnetic fields," *Chinese Optics Letters*, Vol. 12, No. 10, 101601–101605, 2014.
17. Moccia, M., G. Castaldi, V. Galdi, A. Alu, and N. Engheta, "Optical isolation via unidirectional resonant photon tunneling," *Journal of Applied Physics*, Vol. 115, No. 4, 043107, 2014.
18. Born, M. and E. Wolf, *Principles of Optics*, Cambridge University Press, Cambridge, 1999.
19. Gurevich, A. G. and G. A. Melkov, *Magnetic Oscillations and Waves*, Fizmatlit, Moscow, 1994.
20. Krupička, S., *Physik der Ferrite und der verwandten magnetischen Oxide*, Vieweg+Teubner, Braunschweig, 1973.